forests

MDPI

Article

A Multi-Baseline Forest Height Estimation Method Combining Analytic and Geometric Expression of the RVoG Model

Bing Zhang [1,2], Hongbo Zhu [1], Weidong Song [1,2], Jianjun Zhu [3,*], Jiguang Dai [1], Jichao Zhang [1] and Chengjin Li [4]

[1] School of Geomatics, Liaoning Technical University, Fuxin 123000, China; zhangbing@lntu.edu.cn (B.Z.); 47211053@stu.lntu.edu.cn (H.Z.); lntu_swd@163.com (W.S.); daijiguang@lntu.edu.cn (J.D.); zhangjichao@lntu.edu.cn (J.Z.)
[2] Collaborative Innovation Institute of Geospatial Information Service, Liaoning Technical University, Fuxin 123000, China
[3] School of Geosciences and Info-Physics, Central South University, Changsha 410083, China
[4] Guangzhou Urban Planning & Design Survey Research Institute Co., Ltd., Guangzhou 510060, China; lichengjin@gzpi.com.cn
* Correspondence: zjj@csu.edu.cn; Tel.: +86-731-8883-6931

Abstract: As an important parameter of forest biomass, forest height is of great significance for the calculation of forest carbon stock and the study of the carbon cycle in large-scale regions. The main idea of the current forest height inversion methods using multi-baseline P-band polarimetric interferometric synthetic aperture radar (PolInSAR) data is to select the best baseline for forest height inversion. However, the approach of selecting the optimal baseline for forest height inversion results in the process of forest height inversion being unable to fully utilize the abundant observation data. In this paper, to solve the problem, we propose a multi-baseline forest height inversion method combining analytic and geometric expression of the random volume over ground (RVoG) model, which takes into account the advantages of the selection of the optimal observation baseline and the utilization of multi-baseline information. In this approach, for any related pixel, an optimal baseline is selected according to the geometric structure of the coherence region shape and the functional model for forest height inversion is established by the RVoG model's analytic expression. In this way, the other baseline observations are transformed into a constraint condition according to the RVoG model's geometric expression and are also involved in the forest height inversion. PolInSAR data were used to validate the proposed multi-baseline forest height inversion method. The results show that the accuracy of the forest height inversion with the algorithm proposed in this paper in a coniferous forest area and tropical rainforest area was improved by 17% and 39%, respectively. The method proposed in this paper provides a multi-baseline PolInSAR forest height inversion scheme for exploring regional high-precision forest height distribution. The scheme is an applicable method for large-scale, high-precision forest height inversion tasks.

Keywords: polarimetric interferometric synthetic aperture radar (PolInSAR); forest height; analytic expression; geometric expression

Citation: Zhang, B.; Zhu, H.; Song, W.; Zhu, J.; Dai, J.; Zhang, J.; Li, C. A Multi-Baseline Forest Height Estimation Method Combining Analytic and Geometric Expression of the RVoG Model. *Forests* **2024**, *15*, 1496. https://doi.org/10.3390/f15091496

Academic Editor: Luis A. Ruiz

Received: 21 June 2024
Revised: 8 August 2024
Accepted: 20 August 2024
Published: 27 August 2024

1. Introduction

Forest height is one of the important components of global forest-resource surveying and is of great significance for the study of the global carbon cycle and the estimation of forest biomass [1–4]. Accurate and rapid acquisition of large-scale forest height data contributes positively to large-scale studies of forest biomass acquisition, the water cycle, and atmospheric movement [5–9]. Polarimetric interferometric synthetic aperture radar (PolInSAR) introduces polarization measurement technology on the basis of the traditional InSAR technology. PolInSAR not only has the characteristic of InSAR technology, in that it is sensitive to the height and position of the target scatterers, but also has the characteristic of being sensitive to the biophysical properties and structure of vegetation. As a result,

PolInSAR can be used to distinguish the different scattering mechanisms within the same resolution unit, thus possessing the ability to effectively distinguish the scattering phase centers of the ground surface and the canopy [10–12], and has been widely used in forest height estimation.

The key to accurate forest height inversion based on PolInSAR is to find the polarization modes corresponding to "pure body scattering" and "pure ground scattering". However, these two polarization modes cannot be obtained directly from PolInSAR observations due to the depolarization effect of the forest canopy. In view of this, Treuhaft et al. [10–14] proposed the random volume over ground (RVoG) model, which establishes the relationship between the PolInSAR complex coherence coefficients, forest height, the extinction coefficient, and other forest biophysical parameters. At present, the RVoG model and its improved models are the most widely used models in the field of PolInSAR forest height inversion. In 2001, based on the single-baseline PolInSAR configuration, Papathanassiou and Cloude [12] established the correlation between polarization complex coherence and the RVoG model and generalized the inversion of forest height and other parameters based on the RVoG model into a six-dimensional nonlinear system of equations, laying the foundation for the inversion of the forest parameters of PolInSAR. However, the solving of the nonlinear system of equations faces problems, such as the iterative initial value being difficult to determine and the results easily falling into local optima. Therefore, subsequent researchers have successively proposed a series of intelligent optimization algorithms, such as genetic algorithms, back propagation (BP) neural network algorithms, etc. [15–18]. However, these intelligent optimization algorithms, although they have improved the accuracy of the parameter inversion when compared to the traditional nonlinear iterative algorithms, still cannot easily overcome the defects of the nonlinear solving. To address this problem, in 2003, Cloude and Papathanassiou [19] proposed a three-stage method to invert forest height based on the geometric characteristics of the RVoG model expressed as a straight line in the unit circle of the complex plane. However, it has been shown that the three-stage method depends on the accuracy of the straight-line fitting, and high noise causes the accuracy of the straight-line fitting to decrease, resulting in failure of the forest height inversion [20–24]. It can be said that the six-dimensional nonlinear iterative algorithm and the three-stage algorithm are the two most classical single-baseline algorithms in the field of PolInSAR forest height inversion, and they have achieved good forest height inversion results in forest scenarios with a uniform canopy and a flat understory topography [25–27]. However, for most forest scenarios, the forest height inversion accuracy of these two classic algorithms is still insufficient, mainly due to the fact that the PolInSAR observation information provided by the single-baseline configuration is not enough to support unknown parameter inversion based on the RVoG model, and it is necessary to introduce unknown parameter a priori information in order to solve the problem.

Compared to single-baseline PolInSAR forest height inversion, multi-baseline PolInSAR data can obtain rich observation information, which is conducive to forest height inversion. In 2003, Cloude and Papathanassiou [10,19,28] extended the traditional single-baseline three-phase algorithm to a dual-baseline configuration, which solved the limitation of the assumption of a zero amplitude ratio of the ground-to-volume scattering for the body-scattering-dominated polarization approach. However, this method can only consider dual-baseline configurations and is difficult to generalize to other baseline conditions. Meanwhile, the dual-baseline algorithm requires that the two baselines involved in the forest height inversion have certain differences to ensure the accuracy of the forest height inversion [28]. On the other hand, some researchers have focused on selecting the "optimal" baseline among multi-baseline data for forest parameter inversion [23,28–31] in methods such as the optimal elevation accuracy method [29], which judges the quality of the baselines according to the standard deviation of the interferometric phase of the body-scattering-dominant polarization mode. The baseline with the smallest elevation accuracy standard deviation is then selected for the forest parameter inversion. In addition, based on the theory of machine learning, it is also possible to select the optimal observation

geometry for the forest parameter inversion among multiple baselines [30,32,33]. However, the baseline selection criterion considers only a single factor, and it is difficult to determine a baseline selection method that is applicable to all experimental regions, which makes it difficult to map forest height on a large scale. In addition to the above research work, Zhu et al. [6,34–38] explained forest height inversion based on the RVoG model framework from the perspective of measurement adjustment; however, for this method, there are too many unknown parameters, it is difficult to solve, and it fails to take into account optimal baseline selection and irrational baseline exclusion, so it has limited practical application.

In this paper, aiming at the above problems, we propose a multi-baseline forest height estimation method combining analytic and geometric expression of the RVoG model in order to ensure that the rich observation data in the multi-baseline data can be fully utilized to solve the problem of insufficient observation information in the parameter solving. At the same time, the proposed method reduces the uncertainty of the accuracy of the forest height inversion results brought by baselines that are greatly affected by noise and geometrically non-optimal baselines. The specific process is as follows: (1) According to the method of optimal geometrical structure of the coherence region shape, an optimal baseline in the multi-baseline dataset is selected as a reference baseline and all the other baselines are considered to be geometrically constrained baselines. (2) For the reference baseline, a functional model is constructed based on analytic expression of the RVoG model, considering the complex coherence coefficients as observations, and the vegetation biophysical parameters, such as the forest height and extinction coefficient, as the parameters to be solved. (3) For the geometrically constrained baselines of the PolInSAR observations, straight-line fitting is performed based on the geometric expression of the RVoG model, and then the geometric constraints are constructed. The sum of squares of the distances from the expected value of the pure body decoherence coefficients to the fitted straight line is minimized so as to make them participate in the forest height inversion at the same time. Finally, the algorithm proposed in this paper was experimentally validated using PolInSAR data covering the Krycklan coniferous forest experimental area and the Mabounie tropical rainforest experimental area.

The rest of the paper is organized as follows: Section 2 describes the theoretical foundation of this paper. Section 3 explains the research methodology, including the optimal baseline selection method based on the geometric structure of the coherence region shape and the constraint construction method based on geometric expression of the RVoG model. Section 4 presents the experimental results. Section 5 discusses the experimental results obtained in the coniferous forest region as well as the limitations and future studies. Section 6 concludes and summarizes the current work.

2. RVoG Forest Height Inversion Model

2.1. RVoG Model

Inversion of vegetation biophysical parameters, such as forest height, using PolInSAR techniques presupposes the establishment of a correlation between the PolInSAR complex coherence coefficients (PolInSAR observations) and the vegetation biophysical parameters [10].

In the framework of the RVoG model, the forest scene is abstracted as a two-layer structure consisting of the vegetation layer and the ground surface layer in which the scattering particles in the vegetation layer are uniformly random and the spatial distribution obeys the isotropy of each item. The extinction process of the microwave signal in the vegetation layer obeys an exponential function distribution, which can be described by a fixed extinction coefficient. The coverage of the forest canopy extends all the way down to the ground surface layer, and the ground surface layer is the impenetrable plane of the microwave signal. Based on the above assumptions, the RVoG model establishes a correlation between the biophysical parameters of the forest (such as the height of the forest,

the ground phase, and the extinction coefficient) and InSAR coherence which is specifically shown in Equation (1), as follows:

$$\gamma_{(w)} = e^{i\varphi_0} \frac{\gamma_v + \mu_{(w)}}{1 + \mu_{(w)}} \tag{1}$$

where $\gamma_{(w)}$ represents the polarization complex coherence, which contains the coherence amplitude as well as the interferometric phase, and is a PolInSAR observation; φ_0 represents the surface phase, which is related to the surface layer and is an unknown parameter; w represents the polarization mode; and $\mu_{(w)}$ represents the amplitude ratio of the ground-to-volume scattering corresponding to the w polarization mode. According to the definition of the amplitude ratio of the ground-to-volume scattering, it determines the degree of contribution of ground-scattering and body-scattering in the same resolution cell. When $\mu_{(w)} = 0$, this indicates that there is no contribution in regard to ground-scattering from this polarization mode and it is a pure body-scattering polarization mode; conversely, when $\mu_{(w)} = \infty$, this indicates that there is no contribution of body-scattering from this polarization mode and it is a pure ground-scattering polarization mode.

γ_v represents the decoherence factor of the vegetation body caused by the forest canopy structure, which does not contain the contribution of surface scattering but only forest canopy information, such as the forest height and vertical structure of the forest. The specific expression is shown in Equation (2), as follows:

$$\gamma_v = \frac{2\sigma\left(e^{2\sigma h_v / \cos\theta + ik_z h_v} - 1\right)}{(2\sigma + ik_z \cos\theta)\left(e^{2\sigma h_v / \cos\theta} - 1\right)} \tag{2}$$

where h_v represents the forest canopy thickness, i.e., the forest height parameter; θ is the angle of incidence; i is a complex symbol, which is unknown; σ represents the extinction coefficient, which is related to the frequency of the microwave signal, the density of the forest canopy, the dielectric constant, the geometric structure, the nature of forest leaves, and is an unknown parameter; and k_z represents the effective wave number in the vertical direction, which has already been mentioned in the previous section and is related to the InSAR geometry, microwave frequency, and other parameters. In this study we found that k_z has an important role in PolInSAR forest height inversion. Under the premise of the same forest height, different values of k_z have different sensitivity to body decoherence, and choosing the appropriate value of k_z for forest height inversion can ensure the accuracy of the forest height inversion results. The expression of forest height inversion is shown in Equation (3) [10,39,40], as follows:

$$k_z = \frac{4\pi B_\perp}{\lambda R \sin\theta} \tag{3}$$

where $B_\perp$ represents the vertical baseline length, which is a known parameter; λ represents the wavelength of the microwave signal, which is a known parameter; θ represents the incidence angle of the microwave signal, which is a known parameter; and R represents the distance between the radar transmitting antenna and the target, which is a known parameter. The physical significance of the RVoG model, constructed as a function of the PolInSAR polarization complex coherence and the forest parameters by means of an analytical expression, is clear.

2.2. Coherence Loci of the RVoG Model under Multi-Baseline Conditions

The coherence loci is defined as the curve described by the variation in the interferometric complex coherence with the parameters of the physical scattering model [10], as shown in Figure 1. In Figure 1, "Im" is the imaginary part of the complex number, "Re" is the real part of the complex number, "hg" represents the surface elevation, and "a" is the long axis of the ellipse. For the RVoG model, the expression of the RVoG model in

the framework of PolInSAR is shown in Equation (1). Equation (1) is first rewritten as Equation (4), as follows:

$$\begin{aligned} \gamma_{(w)} &= e^{i\varphi_0}\frac{\gamma_v(h_v,\sigma)+\mu_{(w)}}{1+\mu_{(w)}} \\ &= e^{i\varphi_0}\Big(\gamma_v(h_v,\sigma)+L_{(w)}(1-\gamma_v(h_v,\sigma))\Big) \\ L_{(w)} &= \frac{\mu_{(w)}}{1+\mu_{(w)}} \end{aligned} \tag{4}$$

where $L_{(w)}$ is the only polarization correlation quantity in Equation (4). It is a nonnegative factor and takes values in the range of $0 \le L_{(w)} \le 1$. The physical meaning of $L_{(w)}$ can be understood as the component of the effective surface scattering in the observed signal. When $\mu_{(w)} = 0$, this represents pure body-scattering and, at this time, $L_{(w)} = 0$; when $\mu_{(w)} = \infty$, this represents pure surface scattering and, at this time, $L_{(w)} = 1$.

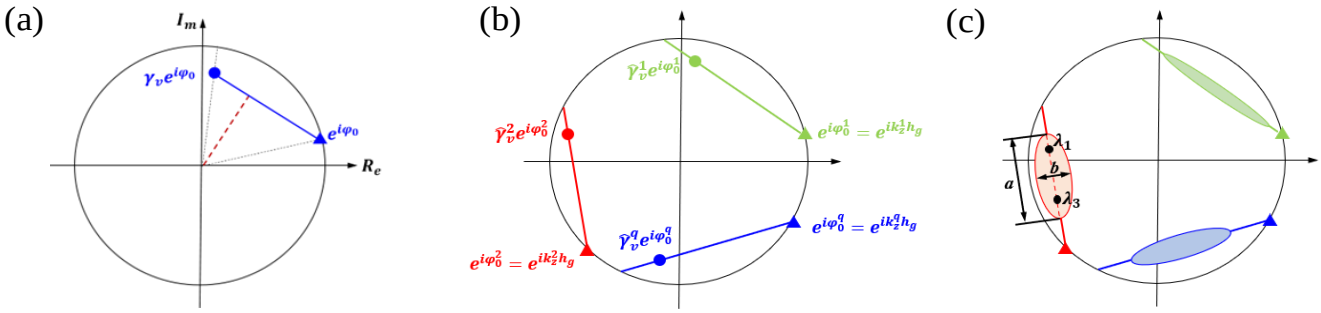

Figure 1. RVoG model coherence loci: (**a**) ideal state RVoG model coherence loci; (**b**) ideal state RVoG model multi-baseline coherence loci; (**c**) real state RVoG model multi-baseline coherence loci.

According to Equation (2), the pure body decoherence coefficient γ_v is a polarization-independent fixed complex value. Equation (4) can then be considered as a straight line equation in the complex plane, and the straight line passes through the two points $e^{i\varphi_0}\gamma_v$ and $e^{i\varphi_0}$ in the complex plane at constant intervals, as shown in Figure 1. Therefore, the coherence loci of the RVoG model is a straight line. Theoretically, the polarization complex coherence coefficients corresponding to each polarization mode should be located on the coherence loci of the RVoG model.

Note that, in practice, not all of the lines shown in Equation (4) are visible and the range of visible line segments depends on the range of values of the amplitude ratio of the ground-to-volume scattering $\mu_{(w)}$. Specifically, in a real case, the range of visible line segments of the coherent trace of the RVoG model corresponds to the variation in the value of $L_{(w)}$ from the minimum value of the amplitude ratio of the ground-to-volume scattering $\mu_{\min}$ to the maximum value of the amplitude ratio of the ground-to-volume scattering $\mu_{\max}$. The visible line segments of the coherent trace of the RVoG model are not all visible. In addition, since the body decoherence factor is expressed in the RVoG model in a complex form, and its phase and amplitude change with the polarization mode, the coherence loci of the RVoG model are not radial rays starting from the origin, such as the blue line segment in Figure 1. The geometric significance of the RVoG model lies in the way the physical baseline is transformed into a visual linear representation, which is more intuitive for baseline selection.

2.3. Amplitude Ratio of the Ground-to-Volume Scattering Parameter Analysis

Based on the framework of the RVoG model, the surface scattering of microwave signals with different polarization modes is related to the polarization modes during the process of penetrating the forest canopy to reach the ground and then scattering. The return signals with different polarization modes contain different ground-scattering information, while the amplitude ratio of the ground-to-volume scattering parameter is polarization-dependent and expresses the ratio of the ground-scattered contribution energy

to the body-scattered contribution energy in the return signals with different polarization modes. The geometric interpretation of the amplitude ratio of the ground-to-volume scattering parameter on the unit circle of the complex plane can be understood as the role of distinguishing the different positions of the complex coherence coefficients corresponding to the different polarization modes on the coherent straight line of the RVoG model. There exists a certain linear correlation between the polarization complex coherence coefficients corresponding to different polarization modes. Since the amplitude ratio of the ground-to-volume scattering parameter cannot determine the role of the position of the coherent straight line of the RVoG model, it can be assumed that the introduction of the amplitude ratio of the ground-to-volume scattering parameter into the modeling process of the RVoG model is an over-parameterization or a redundant parameter introduced for the purpose of distinguishing between different polarization modes.

Since there exists a certain linear relationship between the complex coherence coefficients of different polarizations, it is clear that there is a corresponding linear correlation between their corresponding amplitude ratios from the ground-to-volume scattering. Furthermore, according to the single-baseline RVoG model coherence loci, as shown in Figure 2a, the amplitude ratio of the ground-to-volume scattering can be calculated using Equations (5) and (6) [10,27], as follows:

$$\mu_{(w)} = \frac{F(w)}{1 - F(w)} \tag{5}$$

$$F(w) = \frac{\left|\gamma_{(w)} - \gamma_v\right|}{\left|e^{i\varphi_0} - \gamma_v\right|} = \frac{d_0}{D_0} \quad 0 \le F(w) \le 1 \tag{6}$$

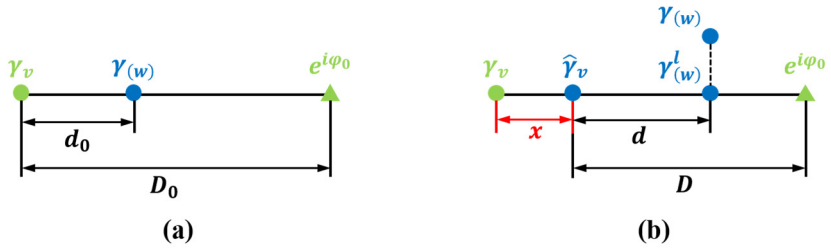

Figure 2. Normalized schematic of the ground-to-volume scattering amplitude ratio. (**a**) Schematic in the theoretical state; (**b**) Schematic in the natural state.

When the arbitrary polarization complex coherence coefficient $\gamma_{(w)}$, the pure body decoherence coefficient γ_v, and the surface phase φ_0 are known, the amplitude ratio of the ground-to-volume scattering can be calculated according to Equations (5) and (6). However, in practice, the pure body decoherence coefficient cannot be obtained directly by observation and the arbitrary polarization mode complex coherence coefficient will deviate from the theoretical straight line due to the influence of temporal decoherence, noise, and other factors. Then, as in Figure 2b, we let the distance from the body-scattering-dominant polarization mode $\hat{\gamma}_v$ to the pure body decoherence coefficient γ_v be x. The arbitrary polarization mode amplitude ratio of the ground-to-volume scattering can then be obtained by Equation (7), as follows:

$$\hat{F}(w_p) = \frac{\left|\hat{\gamma}^l_{(w_p)} - \hat{\gamma}_v\right| + x}{\left|e^{i\varphi_0} - \hat{\gamma}_v\right| + x} = \frac{d_{(w_p)} + x}{D + x} \quad 0 \le \hat{F}(w_p) \le 1 \tag{7}$$

where $\hat{\gamma}^l_{(w_p)}$ represents the point of projection of the observed polarization complex coherence coefficient $\gamma_{(w_p)}$ on the fitted line and $\hat{\gamma}_v$ represents the polarization complex coherence coefficient of the body-scattering-dominated channel.

Under the multi-baseline PolInSAR condition, we first assume that the forest scene attributes remain smooth and unchanged during the data collection. The amplitude ratios of the ground-to-volume scattering of the different baselines corresponding to the same polarization mode then remain consistent so that Equations (8) and (9), when $d_{(w)} = 0$, are as follows:

$$\mu_{(w_p)} = \frac{\hat{F}(w_p)}{1 - \hat{F}(w_p)} = \frac{d_{(w_p)} + x}{D - d_{(w_p)}} \tag{8}$$

$$\frac{x^1}{D^1} = \frac{x^2}{D^2} = \cdots = \frac{x^q}{D^q} = \cdots \tag{9}$$

Combining Equations (8) and (9), the expression of the arbitrary ground–body magnitude ratio under a multi-baseline configuration is as shown in Equation (10), when the forest scene attributes are kept smooth and unchanged during the data collection process. Clearly, according to Equation (10), the ground–body magnitude ratio parameter can still be replaced by the unique unknown x^1 as the number of baselines, as well as the number of polarization modes, increases in the model-based forest height inversion.

$$\mu_{(w_p^q)} = \frac{d_{(w_p^q)} + x^1 D^q / D^1}{D^q - d_{(w_p^q)}} \tag{10}$$

where q represents the qth baseline and x^1 represents the distance from the baseline "1" body-scattering-dominant polarization mode $\hat{\gamma}_v^1$ to the corresponding pure body decoherence coefficient γ_v^1. Theoretically, any interferometric baseline can be designated as baseline "1" and it can be decided on a case-by-case basis which baseline is baseline "1".

2.4. Cloude's Dual-Baseline Forest Height Inversion Algorithm

For forest height inversion based on the traditional three-stage algorithm, the algorithm requires the existence of a polarization channel corresponding to an amplitude ratio of the ground-to-volume scattering of close to 0. However, this assumption is usually difficult to satisfy, especially for forest height estimation based on low-frequency radar waves where the ground-scattering contribution exists in any one of the polarization modes due to their strong penetrative ability. To address this limitation, Cloude and colleagues proposed a dual-baseline PolInSAR forest height inversion algorithm [10,19,28] which eliminates the zero amplitude ratio of the ground-to-volume scattering assumption by constraining the other baseline by the first baseline to estimate the pure body coherence without a ground contribution, as shown in Figure 3.

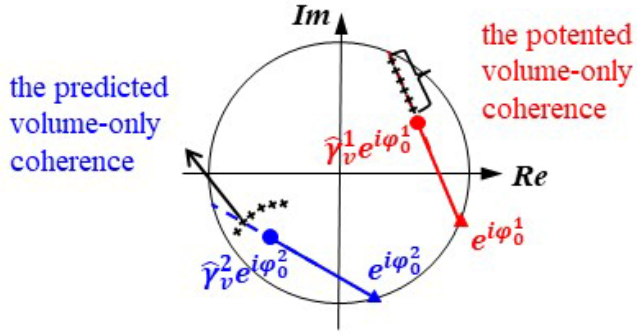

Figure 3. Schematic diagram of the dual-baseline forest height inversion algorithm.

The main algorithmic flow includes:

(1) Straight-line fitting: for two interferometric baselines, B^{ref} and B^1, a straight line is fitted in the respective complex planes using a certain number of complex coherences of the same polarization mode under the baselines.

(2) Surface phase estimation: the surface phases ϕ_0^{ref} and ϕ_0^1 under the respective baselines are estimated according to the coherence order decision criterion in the single-baseline three-stage algorithm.

(3) Estimation of possible solutions for forest height based on baseline B^{ref}: The multiple possible solutions for pure body coherence are selected along the fitted straight line, starting from the assumed point of pure body coherence at a certain step size, up to the point where the straight line intersects with the distal end of the unit circle ground surface. Then, using these possible solutions, their corresponding forest height and extinction coefficient phase combination solutions are successively calculated by building a look-up table.

(4) Forest height estimation: based on the body coherence theoretical Equation (2) in the RVoG model and the vertical wave number of the second baseline B^1, the set of pure body coherence feasible solutions corresponding to the forest height and extinction coefficient combination solutions computed on the basis of the baseline B^{ref} is calculated under the second baseline, as shown as follows in Equation (11):

$$\gamma_{predicted} = e^{j\varphi_0^1}\gamma_v\left(h_v, \sigma, k_z^{B^1}\right) \tag{11}$$

The optimal point corresponding to pure body coherence should minimize the vertical distance from the fitted straight line corresponding to baseline B^1 from a numerical and computational point of view. The set of forest heights and extinction coefficients corresponding to the optimal points are the forest heights estimated by Cloude's double baseline algorithm. Assuming that the second fitted straight line is $y = Mx + C$, the estimation criterion can be expressed as shown as follows in Equation (12):

$$\min_{h_v,\sigma} \frac{1}{1+M^2}\left|\mathrm{Im}\left(\gamma_{predicted}\right) - C - M\mathrm{Re}\left(\gamma_{predicted}\right)\right| \tag{12}$$

Note that the Cloude dual-baseline algorithm requires that the two baselines involved in the forest height inversion have certain differences to ensure the accuracy of the forest height inversion. At the same time, in the case of multiple baselines, this approach can only select two of the baselines for the forest height inversion, which fails to make full use of the rich observation data of the multi-baseline configuration.

3. The Proposed Multi-Baseline Forest Height Estimation Method

When forest height inversion is performed based on multi-baseline PolInSAR data, the observation information is richer, which is favorable for forest height inversion. At the same time, the various error factors in the acquisition process of multi-baseline SAR data will lead to uncertainty in the forest height inversion. As shown in Figure 1c, the elliptical coherence region shape s of the different interferometric baselines has a different eccentricity, which means that the different interferometric baselines are affected by different factors, such as noise; the baselines that are more affected by noise can lead to lower accuracy or even failure of the forest height inversion. In addition, although the multi-baseline PolInSAR configuration can observe the forest scene from multiple angles, an inappropriate observation geometry will also bring about forest height inversion bias. Careful selection of the observation geometry is thus required. Therefore, the existing multi-baseline algorithms mainly focus on baseline selection, and, for a single pixel, this is still essentially single-baseline forest height inversion, which fails to utilize the rich multi-baseline observation data. On the other hand, although the dual-baseline algorithm solves the problem regarding insufficient observation information in forest height inversion, it is difficult to extend it to multi-baseline configurations.

In view of this, we built on the idea of the dual-baseline forest height inversion algorithm proposed by Cloude, as described in Section 2.4, and extended it to the field of multi-baseline forest height inversion, as shown as follows in Figure 4:

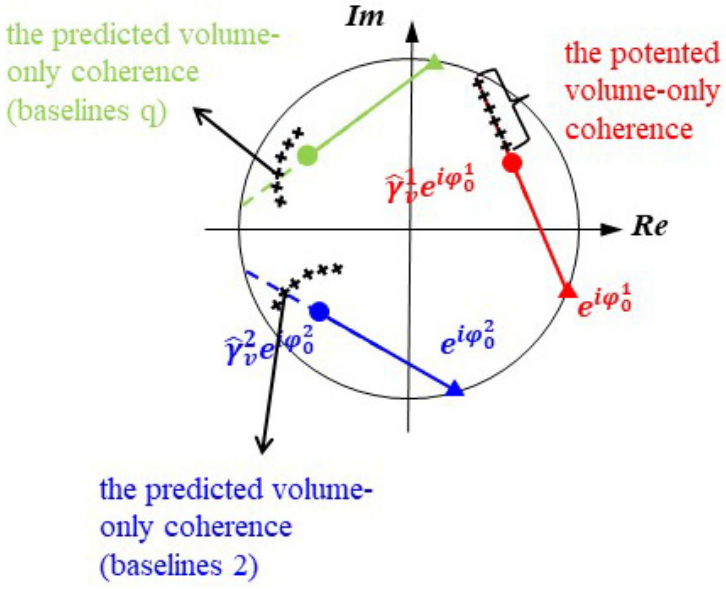

Figure 4. Schematic diagram of the multi-baseline forest height inversion algorithm.

Specifically, in the proposed method, we combine optimal baseline selection with the utilization of multi-baseline observation information. Firstly, the optimal baseline (taking into account the observation quality and interference geometry) is selected and the inverted forest height is expressed by the RVoG model function. For the other baselines which are slightly more affected by noise, as well as the geometrically non-optimal baselines, the observation information of these baselines is transformed into a geometric constraint condition according to the geometric expression of the RVoG model. The algorithm proposed in this paper can not only ensure that the rich observation data in the multi-baseline data can be fully utilized to solve the problem of insufficient observation information in the parameter solving but can also reduce the uncertainty in the accuracy of the forest height inversion results brought by baselines that are greatly affected by noise and the geometrically non-optimal baselines, as shown in the following section.

3.1. Optimal Baseline Selection Based on Coherence Region Shape Geometry

According to Section 2.2, we here define the shape of the coherence region as ellipsoid-like, as in Figure 5. The geometry of the ellipse can then be used as a mixed criterion for the quality of the observed data of this baseline as well as the merit of the observation geometry. That is, for the reference baseline selection criterion, the larger the ellipse eccentricity, the higher the ellipse linearity and the higher the accuracy of the parameter estimation; conversely, the smaller the eccentricity of the ellipse, the lower the ellipse linearity and the lower the accuracy of the parameter inversion. The baseline with the largest elliptical eccentricity can be used as the reference baseline [27]. Specifically, the reference baseline is selected as follows:

Equation (13) can be obtained from the polarization interference matrix T_6, as follows:

$$T_6 = \begin{bmatrix} \langle T_{11} \rangle & \langle \Omega_{12} \rangle \\ \langle \Omega_{12}^{*T} \rangle & \langle T_{22} \rangle \end{bmatrix} \tag{13}$$

where $*T$ represents the conjugate transpose of the matrix and T_{11}, T_{22}, Ω_{12} are matrices of 3×3. The new complex matrix Π can be redefined according to T_{11}, T_{22}, Ω_{12}, as shown as follows in Equation (14):

$$\begin{aligned} \Pi &= \sqrt{T^{-1}}\Omega_{12}\sqrt{T^{-1}} \\ T &= \tfrac{1}{2}(T_{11} + T_{22}) \end{aligned} \tag{14}$$

The Schur decomposition of the complex matrix A yields the following Equation (15):

$$\Pi = [U]^{*T}[R][U] = [U]^{*T}\begin{bmatrix}\lambda_1 & \delta_{12} & \delta_{13}\\ 0 & \lambda_2 & \delta_{23}\\ 0 & 0 & \lambda_3\end{bmatrix}[U] \tag{15}$$

From the Schur decomposition, it can be seen that the eigenvalues in matrix R can be arbitrarily combined into three groups of elliptic parameters. In the proposed approach, this group of parameters λ_1, λ_2, δ_{13} is selected for the elliptical coherence region shape of the centroid. The elliptical coherence region shape of the length of the long axis a, the length of the short axis b, as well as the elliptical coherence region shape of the centroid rate of the Eccentricity (Ecc) can be calculated from Equations (16) and (17), as follows:

$$\begin{aligned} a &= \sqrt{|\lambda_1 - \lambda_3|^2 + |\delta_{13}|^2}\\ b &= |\delta_{13}| \end{aligned} \tag{16}$$

$$Ecc = \sqrt{1 - \left(\frac{b}{a}\right)^2} \tag{17}$$

When Q interferometric baselines exist, the Ecc of the elliptical coherence region shape corresponding to each baseline is calculated separately. The reference baseline selection criterion can then be expressed by Equation (18), where max‖ ‖ stands for taking the maximum value of the matrix.

$$Ecc^{ref} = \max\left\| \begin{matrix} Ecc^1 \\ Ecc^2 \\ \vdots \\ Ecc^q \\ \vdots \\ Ecc^Q \end{matrix} \right\| \tag{18}$$

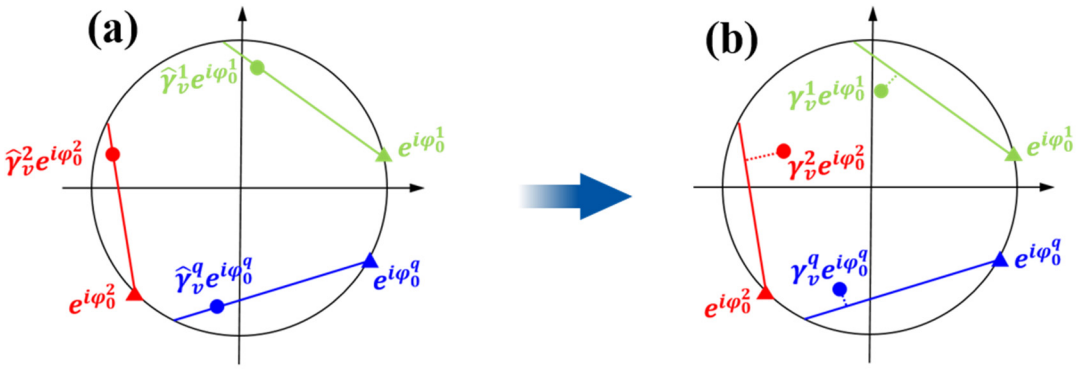

Figure 5. Geometric constraint construction method based on the RVoG model. (**a**) Schematic in the theoretical state; (**b**) Schematic in natural state.

3.2. Constraint Construction Based on Geometric Expression of the RVoG Model

Based on the multi-baseline PolInSAR configuration, multiple fitted straight lines can be observed in the unit circle of the complex plane, as shown in Figure 5a. Theoretically, the "pure body decoherence coefficient" points related to vegetation biophysical parameters such as forest height and the extinction coefficient should be located on the fitted straight line, where the distance from the pure body decoherence point to the fitted straight line is 0. However, due to the influence of various factors such as observation noise, data processing, etc., the pure body decoherence coefficient points in the actual situation may deviate from the fitted straight line. As shown in Figure 5b, there exists a certain perpen-

dicular distance between the pure body decoherence coefficients corresponding to each geometrically constrained baseline and the corresponding fitted straight line d. Accordingly, in the proposed approach, we construct a restriction based on the geometric expression of the RVoG model as follows: within the unit circle of the complex plane, the sum of the squared distances between the pure body decoherence coefficients corresponding to each geometrically constrained baseline and the corresponding fitted straight line is minimized.

Assuming that Q interferometric baselines exist, the geometric constraint baseline is $Q-1$. Also, assuming that the equation of the geometric constraint baseline fitting a straight line in the unit circle of the complex plane can be expressed as $\mathrm{Im} = M_q \mathrm{Re} + C_q$, the specifics of the geometric constraints are as shown as follows in Equations (19)–(21):

$$d_2^2 + d_3^2 + \cdots + \cdots d_q^2 + \cdots + d_Q^2 = 0 \tag{19}$$

$$d_q = \frac{1}{1+M_q^2}\left|\mathrm{Im}\left(\gamma_v^q\right) - C_q - M_q \mathrm{Re}\left(\gamma_v^q\right)\right| \tag{20}$$

$$\gamma_v^q = \frac{2\sigma\left(e^{2\sigma h_v/\cos\theta + ik_z^q h_v} - 1\right)}{\left(2\sigma + ik_z^q \cos\theta\right)\left(e^{2\sigma h_v/\cos\theta} - 1\right)} \tag{21}$$

where the subscript of d_q, C_q, M_q represents the geometric constraint baseline labeling; q represents the qth geometrically constrained baseline; d_q represents the perpendicular distance from the pure body decoherence coefficient corresponding to the qth geometrically constrained baseline to the corresponding fitted straight line; Re( ): represents taking the real part of the complex number; Im( ): represents taking the imaginary part of the complex number; M_q represents the slope of the geometrically constrained baseline corresponding to the equation of the fitted straight line in the unit circle of the complex plane, which can be obtained by fitting a straight line in the first step of the three-stage algorithm [19]; and C_q represents the intercept of the geometrically constrained baseline corresponding to the equation of the fitted straight line in the unit circle of the complex plane, which can be obtained by fitting a straight line in the first step of the three-stage algorithm [19].

Note that the pure body decoherence coefficient points cannot be obtained directly from observations. Therefore, in the proposed approach, we adopt the approach of obtaining the mathematical expectation value instead of the true value to construct the constraints based on Equation (19). Since the pure body decoherence coefficient is related to vegetation biophysical parameters such as forest height and extinction coefficient, the above two parameters are unknown. In the proposed approach, we choose to calculate the expected value of the pure body decoherence coefficient using Equation (22) and use it to construct the above constraints instead of the theoretical value of the pure body decoherence coefficient.

$$\hat{\gamma}_v^q = \frac{2\hat{\sigma}\left(e^{2\sigma\hat{h}_v/\cos\theta + ik_z^q \hat{h}_v} - 1\right)}{\left(2\hat{\sigma} + ik_z^q \cos\theta\right)\left(e^{2\hat{\sigma}\hat{h}_v/\cos\theta} - 1\right)} \tag{22}$$

where $\hat{\gamma}_v^q$ represents the estimate of the pure body decoherence coefficient coming from the geometrically constrained baseline of q; $\hat{h}_v$ represents the estimate of the unknown parameter of forest height; and $\hat{\sigma}$ represents the estimate of the unknown parameter of the extinction coefficient. Accordingly, Equation (19) is converted to Equation (23), as follows:

$$d_q = \frac{1}{1+M_q^2}\left|\mathrm{Im}\left(\hat{\gamma}_v^q\right) - C_q - M_q \mathrm{Re}\left(\hat{\gamma}_v^q\right)\right| \tag{23}$$

According to Equations (22) and (23), the constraints of the PolInSAR forest height inversion algorithm proposed in this paper are as shown as follows in Equation (24):

$$\min\left\|d_2^2 + d_3^2 + \cdots + \cdots d_q^2 + \cdots + d_Q^2\right\| \tag{24}$$

3.3. Multi-Baseline PolInSAR Forest Height Inversion with Additional RVoG Model Geometric Constraints

3.3.1. Multi-Baseline Function Expression for RVoG Modeling

The RVoG model in multi-baseline mode with the PolInSAR configuration can be expressed as shown in Equation (25), as follows:

$$\hat{L} = L + V = f_{RVoG}\left(\hat{h}_v, \hat{\sigma}, \hat{\varphi}_0^q, \hat{x}^{ref}\right) \tag{25}$$

where $\hat{x}^{ref}$ represents the normalized parameter estimate of the amplitude ratio of the ground-to-volume scattering corresponding to the reference baseline. From Equation (25), it can be seen that the surface phase φ_0^q parameter is the only baseline-correlated parameter. That is, based on the multi-baseline PolInSAR framework, the differences existing in the interferometric geometries of the different baselines lead to the baseline correlation of the surface phase. On the other hand, the surface elevation does not change with the baseline change, so the baseline-correlated surface phase can be considered to be converted to the unique baseline-uncorrelated surface elevation through the phase-to-elevation conversion relationship, as shown in Figure 6. In the multi-baseline configuration, assuming that there are Q interferometric baselines, the Q surface phase φ_0 parameters can be reduced to one surface elevation parameter h_g using Equation (26). Based on the above, Equation (25) can be rewritten as Equation (27).

$$h_g = \frac{\varphi_0^q}{k_z^q} \quad q = 1,\ 2, \cdots,\ Q \tag{26}$$

$$\hat{L} = L + V = f_{RVoG}\left(\hat{h}_v, \hat{\sigma}, h_g, \hat{x}^{ref}\right) \tag{27}$$

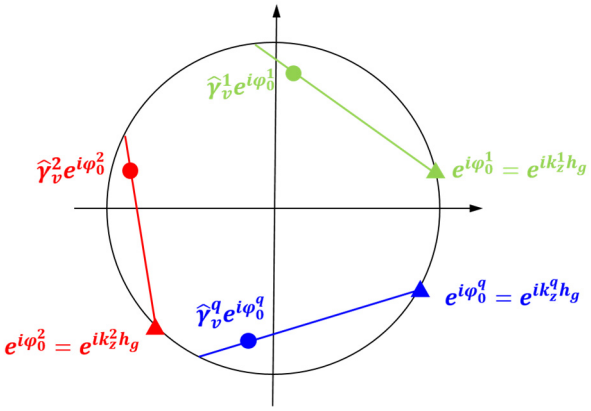

Figure 6. Schematic diagram of the conversion of surface phases to surface elevations; superscripts 1, 2, and q in the figure indicate baselines.

3.3.2. Multi-Baseline Forest Height Inversion Functional Model for Joint RVoG Model Analysis and Geometric Expression

Under the multi-baseline PolInSAR configuration, we first select one of the baselines as the reference baseline, according to the method described in Section 3.1, and then perform the forest height inversion calculation based on the expression of the RVoG function. The observation data of all the other baselines are converted into constraints, as described in Section 3.2, and then the functional model of the PolInSAR forest height inversion

algorithm, taking into account the constraints of the multiple baselines, can be expressed as shown in Equation (28), as follows:

$$\begin{cases} \hat{L} = L + V = f_{RVoG}\left(\hat{h}_v, \hat{\sigma}, \hat{h}_g, \hat{x}^{ref}\right) \\ d_1^2 + d_2^2 + \cdots + \cdots d_q^2 + \cdots + d_{Q-1}^2 = 0 \\ d_q = \frac{1}{1+M_q^2}\left|\mathrm{Im}\left(\hat{\gamma}_v^q\right) - C_q - M_q \mathrm{Re}\left(\hat{\gamma}_v^q\right)\right| \\ \hat{\gamma}_v^q = \frac{2\hat{\sigma}\left(e^{2\hat{\sigma}\hat{h}_v/\cos\theta + ik_z^q\hat{h}_v} - 1\right)}{\left(2\hat{\sigma} + ik_z^q\cos\theta\right)\left(e^{2\hat{\sigma}\hat{h}_v/\cos\theta} - 1\right)} \end{cases} \tag{28}$$

When the number of observations in Equation (28) is greater than the number of unknown parameters, joint RVoG model analysis and geometric expression of the multi-baseline forest height inversion can be performed.

In the proposed approach, based on the idea of measurement adjustment, the forest height and extinction coefficient are regarded as indirect leveling problems with constraints in the complex domain. Using the functional model, the proposed approach adopts the leveling criterion of minimizing the sum of squares of the modes of the complex residual values to construct the complex least squares leveling algorithm for parameter solving. In addition, due to the difficulty of linearizing the RVoG model, the proposed approach still adopts the nonlinear least squares iterative method for parameter solving.

3.3.3. Forest Height Estimation Using Nonlinear Least Squares Optimization

Under the multi-baseline configuration, assuming that there are Q baselines and P polarization modes for each baseline, a nonlinear least-square optimization algorithm is employed to solve the parameters. The corresponding objective function is shown as follows in Equation (29):

$$\begin{cases} \min\left(\sum_{q=1,p=1}^{Q,P}\left|\gamma^q(\omega_p) - \hat{\gamma}^q(\omega_p)\right|\right) \\ \min\left\|d_1^2 + d_2^2 + \cdots + \cdots d_q^2 + \cdots + d_{Q-1}^2\right\| \end{cases} \tag{29}$$

The initial values of the surface elevation $\widetilde{h}_{g_0}$, extinction coefficient $\widetilde{\sigma}$, and forest height $\widetilde{h}_0$ are calculated as follows.

Based on the RVoG model, the proposed approach adopts a three-stage algorithm and combines it with the reference baseline selection method described in Section 3.1 to calculate the initial values of surface elevation, extinction coefficient, and forest height. The specific steps are as follows.

Firstly, the reference baseline is selected, based on the multi-baseline PolInSAR framework. The *Ecc* of the elliptical coherence region shape corresponding to each pixel of each baseline is calculated according to each equation from Equation (19) to Equation (23). Then, for each pixel, Equation (24) is used to select the reference baseline corresponding to that pixel.

Secondly, the initial value of the surface elevation $\widetilde{h}_{g_0}$, the initial value of the extinction coefficient $\widetilde{\sigma}$, and the initial value of the forest height $\widetilde{h}_0$ corresponding to each pixel are calculated using the method of calculating the initial value of the unknown parameters described in Section 3.3.2.

The initial value of the normalization parameter x_0 of the amplitude ratio of the ground-to-volume scattering is set to 0, i.e., $\widetilde{x}^{ref} = 0$.

According to experience, the "forest height" obtained by the three-stage algorithm generally lies between one-half of the real forest height and the top of the forest canopy. Therefore, in the proposed approach, we set the forest height iteration range to $0.5\widetilde{h}_0 \leq h_v \leq 1.5\widetilde{h}_0$.

4. Forest Height Inversion in the Mabounie Rainforest Region

4.1. Experimental Data and Preprocessing in the Mabounie

Four PolInSAR images covering the Mabounie area of Gabon in West Africa, which were obtained during the 2016 AfriSAR campaign, were used to experimentally validate the PolInSAR multi-baseline forest height inversion method combining analytic and geometric expression of the RVoG model. The main parameters of the PolInSAR system used in the AfriSAR campaign were as follows: the wavelength was about 69 cm, the polarization mode was HH/HV/VH/VV, the flight altitude was about 6000 m, the azimuthal resolution was 0.9 m, and the oblique distance to resolution was 1.2 m. The basic details of the four PolInSAR images and their constituent interferometric baseline parameters are given in Table 1.

Table 1. PolInSAR data parameters in the experimental area.

Image	Interference with	Temporal Baseline (Days)	Spatial Baseline (Meters)	Vertical Effective Wave Number Range
1	-	Master image	Master image	Master image
2	1	0	0	0.01–0.05
3	2	0	0	0.04–0.10
4	3	0	0	0.06–0.13

4.2. Forest Height Inversion Results and Analysis in the Mabounie

This subsection provides qualitative and quantitative analyses of the forest heights inverted by the proposed PolInSAR inversion algorithm with geometric constraints and the traditional multi-baseline inversion algorithm based on the geometrically optimal structure of the coherence region shape. Figure 7 shows the results of forest height inversion by the two different algorithms and the LiDAR forest height products covering part of the experimental area. Figure 7a shows the forest height inverted by the traditional multi-baseline algorithm; Figure 7b shows the forest height inverted by the algorithm proposed in this paper; and Figure 7c shows the LiDAR forest height products covering part of the experimental area. The forest heights inverted by the algorithm proposed in this paper are basically consistent with the trend of the LiDAR forest height products used as "ground-truth data", while the forest heights inverted by the traditional multi-baseline algorithm are relatively consistent with the LiDAR products in terms of trend; however, there is an underestimation phenomenon in the overall scope.

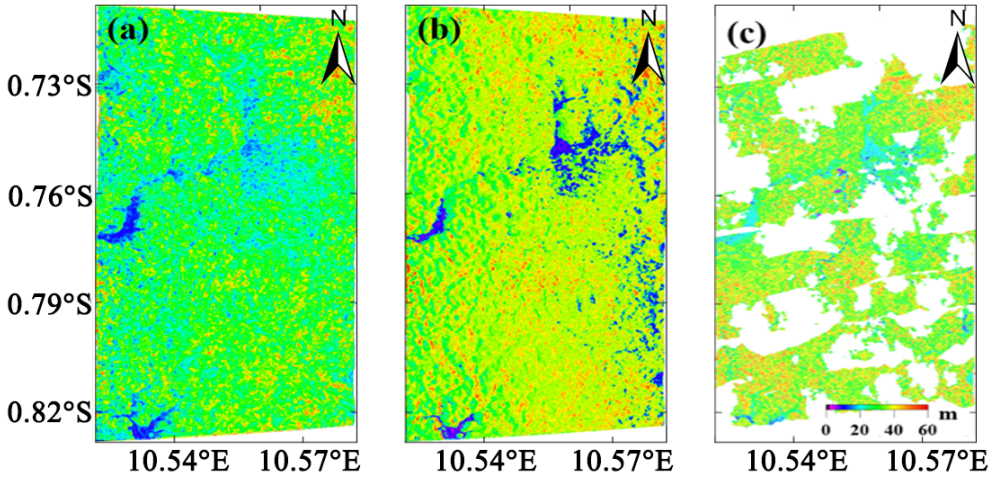

Figure 7. (**a**) The forest height inversion results of the traditional multi-baseline inversion algorithm; (**b**) the forest height inversion results of the algorithm proposed in this paper; (**c**) the LiDAR forest height products that cover a part of the Krycklan coniferous forest region.

In order to quantitatively analyze the forest height inversion accuracy of the algorithm proposed in this paper, LiDAR forest height products covering part of the experimental area were used as reference forest heights. In total, 1170 forest sample plots were first selected in the experimental area. Based on the selected 1170 forest sample plots, these data were used to cross-validate the forest height inversion results shown in Figure 7a as well as Figure 7b. As shown in Figure 8, the accuracy of the forest height inversion results was quantitatively measured using the root–mean–square error (RMSE) values.

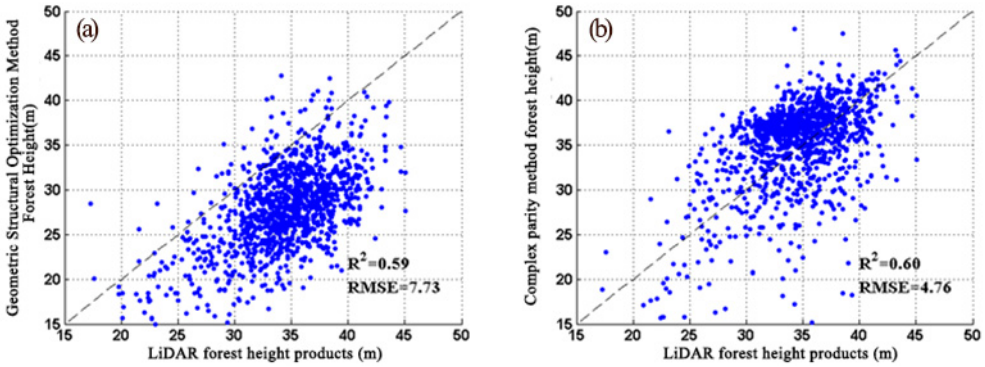

Figure 8. Cross-validation plots of the forest heights inverted by the two different algorithms, with the LiDAR forest height products covering part of the Mabounie rainforest region. (**a**) The results of the traditional multi-baseline inversion algorithm; (**b**) the results of the algorithm proposed in this paper.

According to Figure 8a,b, it is clear that the PolInSAR forest height inversion algorithm proposed in this paper has an obvious advantage over the traditional multi-baseline forest height inversion algorithm in this experimental region. For the proposed algorithm, the scatter points of the cross-validation plots are basically uniformly distributed on the two sides of the reference line (the dotted line shown in the figure). The scatter points of the traditional multi-baseline algorithm are mostly distributed on the lower side of the reference line in the figure, which represents underestimation of the forest height. The RMSE of the forest height inversion results of the proposed algorithm is 4.76 m, while that of the traditional multi-baseline algorithm is 7.73 m. The accuracy of the algorithm proposed in this paper represents an improvement of about 39%. The main reasons for the higher accuracy of the proposed algorithm in forest height inversion are as follows:

(1) The baseline selection criterion for the traditional coherence region shape geometric structure optimization method is to select a baseline that is more "flat and long" in the elliptically polarized coherence region shape. For this experimental area, the flat and long polarized coherence region shape corresponds to interferometric pairs with longer spatial baselines, which correspond to a larger vertical effective wave number k_z. In the high forest region, the coherence–height sensitivity tends to be saturated, which leads to underestimation of the high forest. (2) The PolInSAR forest height inversion algorithm proposed in this paper selects one baseline as the computational baseline, and the other baseline data are transformed into geometric constraints. This approach objectively applies all the feasible observation data for the forest height inversion and solves the problem of rank-loss of forest height inversion based on the RVoG model. The problem regarding forest height inversion based on the RVoG model has been solved, the forest height inversion is more advantageous, and the effect has been found to be superior in this experimental area.

5. Discussion

5.1. Forest Height Inversion in the Krycklan Coniferous Forest Region

5.1.1. Experimental Data and Preprocessing in the Krycklan

A further experimental validation was carried out using four PolInSAR images from the Krycklan experimental area in Sweden; these images constitute three interferometric pairs. The main parameters of the E-SAR P-band airborne SAR system are given in Table 2.

The basic details of the four PolInSAR images and their constituent interferometric baseline parameters are given in Table 3.

Table 2. E-SAR P-band airborne SAR system main parameters.

Band	Wavelength (Centimeters)	Polarization Mode	Flight Altitude (Meters)	Azimuthal Resolution (Meters)	Oblique Distance to Resolution (Meters)
P-band	86	HH/HV/VH/VV	About 3000	0.95	1.50

Table 3. The main details of the Krycklan interferometric pairs.

Image	Interference with	Temporal Baseline (Minutes)	Spatial Baseline (Meters)	Vertical Effective Wave Number Range
1	-	-	-	Master image
2	1	31	16	0.02–0.14
3	2	53	24	0.02–0.20
4	3	70	32	0.05–0.26

Three interferometric baselines were formed, with the image labeled 1 acting as the main image and the images labeled 2, 3, and 4 acting as the auxiliary images. The free SAR data processing software PolSARpro 4.2.0 from the European Space Agency was used to perform the data preprocessing for each interferometric baseline, which included SAR image alignment, flat-earth phase removal, multiview processing, and interferometric processing. The scale of the multiview processing was 2×1 (azimuthal $\times$ distance direction); the coherence estimation window in the interferometric processing step was set to 11×11; and the polarization complex coherence coefficients corresponding to each interferometric baseline were estimated using the following phase diversity (PD) coherence optimization algorithm [10]: $\gamma(PDHigh^1)$, $\gamma(PDHigh^2)$, $\gamma(PDHigh^3)$, $\gamma(PDLow^1)$, $\gamma(PDLow^2)$, $\gamma(PDLow^3)$, with the superscripts 1, 2, and 3 representing the different interferometric baselines and PDHigh and PDLow representing the polarization mode obtained by PD coherence optimization.

After obtaining the polarized complex coherence coefficients, these complex observations could be used to test the effectiveness of the multi-baseline PolInSAR forest height inversion algorithm proposed in this paper. The traditional multi-baseline forest height inversion algorithm based on the geometrically optimal structure of the coherence region shape was used for comparison, and the LiDAR forest height products covering the experimental area were used as ground-truth data for the cross-validation.

5.1.2. Forest Height Inversion Results and Analysis in the Krycklan

The forest height inversion results based on the traditional multi-baseline algorithm and the algorithm proposed in this paper are shown in Figures 9a and 9b, respectively. In addition, Figure 9c shows the LiDAR forest height products in the Krycklan experimental area based on the LiDAR products obtained during the BioSAR 2008 project.

Firstly, a qualitative analysis was carried out. Intuitively, the trend of the forest height results in the Krycklan experimental area is basically the same between the algorithm proposed in this paper and the traditional multi-baseline algorithm. Overestimation of the forest height can be seen on the right side of the forest height inversion results. The main reason for this phenomenon is that, due to the airborne SAR data used in this study, the incidence angle at the far end is larger. This corresponds to a smaller vertical effective wave number, which is insensitive to the change in forest height and has a weaker ability in regard to resisting the noise, which ultimately leads to a certain degree of overestimation of the forest height in the forest height inversion.

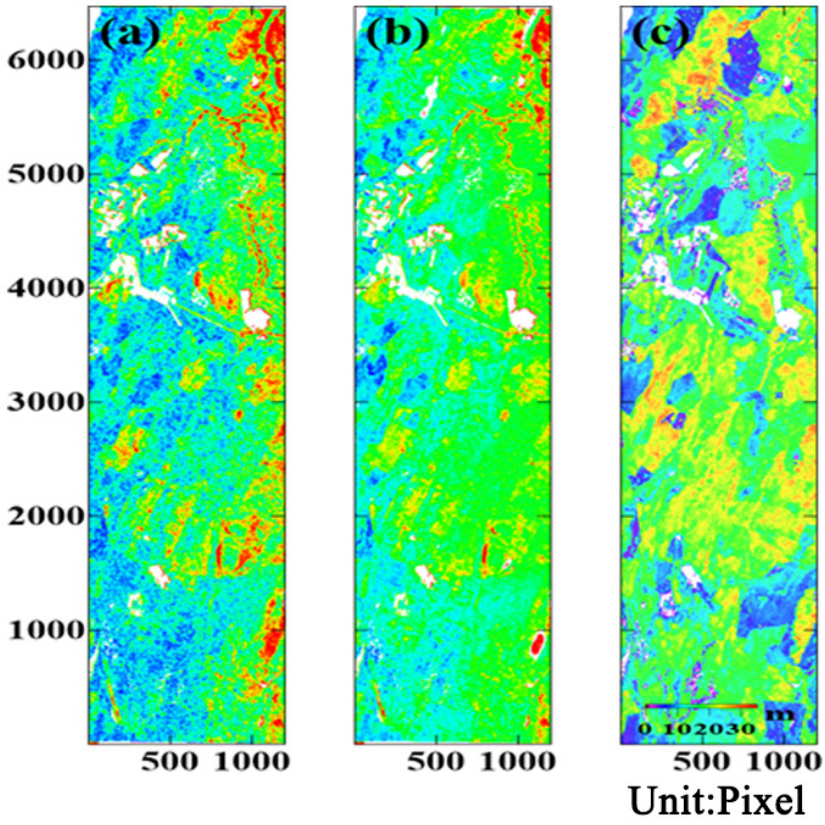

Figure 9. (**a**) The forest height inversion results of the traditional multi-baseline algorithm; (**b**) the forest height inversion results of the algorithm proposed in this paper; (**c**) the LiDAR forest height products covering part of the Krycklan coniferous forest region.

We also quantitatively analyzed the forest heights inverted by the two algorithms with the LiDAR forest height products. We selected 1318 forest sample plots in the study area and calculated the average forest height value corresponding to each sample plot for quantitative verification of the accuracy of the proposed algorithm in forest height inversion. Figure 10 shows the cross-validation plots of the forest heights based on the inversion results of the two algorithms with the LiDAR forest height products. According to Figure 10a,b, the RMSE of the inversion results of the algorithm proposed in this paper and the traditional multi-baseline algorithm are 4.28 m and 5.15 m, respectively. The accuracy of the forest height inversion results of the algorithm proposed in this paper represents an improvement of about 17%.

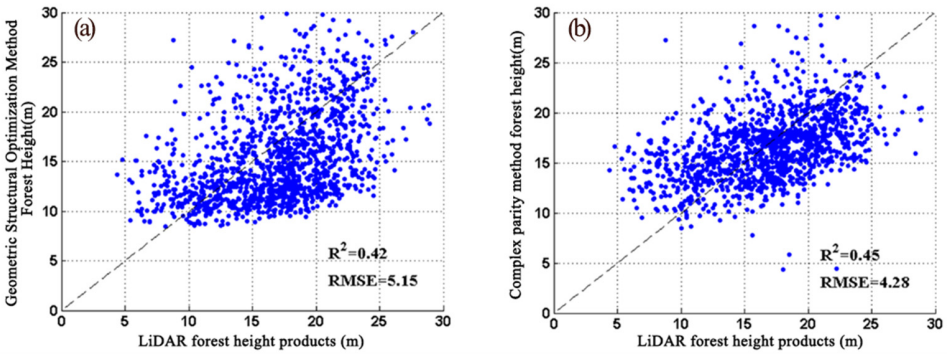

Figure 10. Cross-validation plots of the forest heights inverted by the two different algorithms, with the LiDAR forest height products covering part of the Krycklan coniferous forest region. (**a**) The results of the traditional multi-baseline inversion algorithm; (**b**) the results of the algorithm proposed in this paper.

The reason for the superior accuracy in forest height inversion achieved via the algorithm proposed in this paper is that the traditional multi-baseline algorithm first selects an "optimal" baseline for any pixel in the interferogram and then carries out the forest height inversion based on the single-baseline observation data provided by the "optimal" baseline. Due to the lack of observation information, it is necessary to carry out the forest height inversion based on the assumption of a zero amplitude ratio for the ground-to-volume scattering [19]. Since we adopted P-band SAR data for the real-data experiments, which have a strong penetrative ability, even though the body-scattering-dominant polarization mode (the PDHigh polarization mode adopted in this study) still contains strong ground-scattering signals, the assumption of a zero amplitude ratio for the ground-to-volume scattering is no longer valid, resulting in bias in the forest height inversion.

The algorithm proposed in this paper does not need to assume that the amplitude ratio of the ground-to-volume scattering of a certain polarization channel existing in the reference baseline is zero; however, at the same time, it takes into account the utilization of the rich observation information under the multi-baseline PolInSAR configuration. This approach solves the problem of insufficient observation information for forest height inversion based on the RVoG model and improves the accuracy of the forest height inversion.

Our results are corroborated in the studies of Xie et al. [41] and Zhao et al. [42]. In the study by Xie et al. a multi-baseline decorrelation simultaneously accounts for the ground-scattering contribution, the spatial baseline configuration, and the temporal decorrelation (the main part of the non-volume decorrelation) in a multi-baseline PolInSAR forest canopy height inversion method. The Krycklan region was used as the study area and the accurate spatial distribution of the forest canopy height was obtained. In the study of Zhao et al. they proposed an RVoG model incorporating a hierarchical Bayesian framework to realize the inversion of forest canopy height. In their study, experiments were conducted based on the Krycklan region using P-band data and L-band data, respectively, to obtain the spatial distribution of forest canopy height in the region. In our study, the spatial distribution of forest canopy height in this study area obtained in this paper is similar to that of the two previous researchers, and, compared with their study, we considered the utilization of rich observation information under multi-baseline PolInSAR configuration, thus obtaining a more accurate spatial distribution map of forest canopy height in the Krycklan region.

5.2. Limitations and Future Research

In this paper, we have proposed a multi-baseline forest height estimation method combining the analytic and geometric expression of the RVoG model that makes full use of the rich observation data in the multi-baseline data to carry out forest height inversion. The method makes full use of the rich observation data in the multi-baseline data for forest height inversion and, at the same time, reduces the uncertainty of the accuracy of the forest height inversion results caused by baselines affected by noise and the geometrically non-optimal baselines. However, the method still has some limitations.

In the previously reported studies, research on the selection of optimal baselines has received extensive attention, with methods based on the optimal elevation accuracy, the method of optimal geometric structure, artificial intelligence methods, and other algorithms being examined. However, most of the reported studies on optimal baseline selection have focused on a single-baseline selection criterion, which is more suitable for specific forest height scenarios. When the selected baseline is applied to areas with large differences in the natural environment, its universality needs to be improved. For the proposed algorithm, it only uses the optimal baseline selection method based on the geometric structure of the coherence region shape. In future research, we will focus on the study of an adaptive optimal baseline selection method in order to realize optimal baseline selection for complex natural scenarios.

On the other hand, in the forest height inversion task under multi-baseline conditions, there may be multiple baselines that are suitable for forest height inversion. In this condition, increasing the multi-baseline observations helps to improve the robustness of the forest

height inversion accuracy. For the algorithm proposed in this paper, the optimal baseline selection method based on only the geometric structure of the coherence region shape obtains a single optimal baseline. It ignores the other baselines suitable for forest height inversion and directly uses them as constrained baselines, which, to a certain extent, undermines the richness of the observations brought by the multi-baseline PolInSAR configuration. Therefore, how to design a baseline selection method that selects multiple preferred baselines as computational baselines and uses the remaining suboptimal baselines as constraining baselines will be of concern in our future research.

Furthermore, the accuracy and reliability of forest height inversion based on the PolInSAR technique are closely related to the stability of the forest scatterers and the length of the interferometric baseline. For the dual-station mode, it is not affected by temporal decoherence, but the interferometric baseline selection methodology considers only a single factor, with which it is difficult to cope with the spatial complexity of forest height. For the heavy-track mode, it has the advantage of using multiple interferometric baseline lengths to observe the same target at multiple scales, but the effect of temporal decoherence is unavoidable. The hybrid mode of dual-station + heavy-track not only makes up for the respective disadvantages of each of these modes in forest height inversion but also enhances the accuracy and reliability of PolInSAR-based forest height inversion. It can also improve the update rate for forest height mapping based on PolInSAR technology. For the algorithm proposed in this paper, how to take into account the advantages of the dual-station mode without temporal decoherence and the heavy-track mode with various interferometric baselines is worthy of attention. Furthermore, how to construct a forest height inversion algorithm integrating dual-station + heavy-track PolInSAR modes under the conditions of the different morphological features of the forest, so as to improve the accuracy and robustness of the inversion results, will be one of the goals of our future research.

6. Conclusions

In this study, we considered the problem of the existing multi-baseline forest height inversion methods that mostly use the selection of an optimal baseline without proper consideration of the PolInSAR data quality and observation geometry. For the problem of arbitrary resolution units essentially utilizing only the single-baseline observation information and failing to make full use of the rich multi-baseline observation information, we have proposed a multi-baseline PolInSAR forest height inversion algorithm with additional geometric constraint of the RVoG model. For any pixel in the interferogram, an optimal baseline is selected according to the geometric structure of the coherence region shape, and analytic expression of the RVoG model is used to establish a functional model for the forest height inversion. The other constrained baseline observations are converted to constraints based on the geometric expression of the RVoG model and also participate in the forest height inversion at the same time. The algorithm was validated using P-band PolInSAR data from the Krycklan coniferous forest area and the Mabounie tropical rainforest area. The results showed that, compared with the traditional multi-baseline PolInSAR forest height inversion algorithm based on the optimal geometric structure of the coherence region shape, the accuracy of forest height inversion achieved with the algorithm proposed in this paper in the coniferous forest area and tropical rainforest area was improved by 17% and 39%, respectively.

Author Contributions: Conceptualization, B.Z. and J.Z (Jianjun Zhu).; methodology, B.Z. and H.Z.; software, J.Z (Jichao Zhang). and C.L.; validation, W.S., J.Z. (Jichao Zhang) and B.Z.; formal analysis, B.Z.; investigation, B.Z.; writing—original draft preparation, B.Z.; writing—review and editing, H.Z. and J.D.; visualization, J.Z. (Jichao Zhang); supervision, C.L.; project administration, B.Z.; funding acquisition, B.Z. All authors have read and agreed to the published version of the manuscript.

Funding: This work was supported in part by the National Natural Science Foundation of China under Grant 42204031 and a project funded by the China Postdoctoral Science Foundation (2022MD723791).

Data Availability Statement: The data presented in this study are available on request from the corresponding author.

Acknowledgments: We are very grateful to all the reviewers, institutions, and researchers for their help and advice on our work.

Conflicts of Interest: Author Chengjin Li was employed by the company Guangzhou Urban Planning & Design Survey Research Institute Co., Ltd. The remaining authors declare that the research was conducted in the absence of any commercial or financial relationships that could be construed as a potential conflict of interest.

References

1. Pan, Y.; Birdsey, R.A.; Fang, J.; Houghton, R.; Kauppi, P.E.; Kurz, W.A.; Phillips, O.L.; Shvidenko, A.; Lewis, S.L.; Canadell, J.G.; et al. A large and persistent carbon sink in the world's forests. *Science* **2011**, *333*, 988–993. [CrossRef] [PubMed]
2. Houghton, R.A.; Hall, F.; Goetz, S.J. Importance of biomass in the global carbon cycle. *J. Geophys. Res. Biogeosci.* **2009**, *114*, G2. [CrossRef]
3. Zhang, B.; Zhu, H.; Xu, W.; Xu, S.; Chang, X.; Song, W.; Zhu, J. A Fourier–Legendre Polynomial Forest Height Inversion Model Based on a Single-Baseline Configuration. *Forests* **2024**, *15*, 49. [CrossRef]
4. Zhu, H.; Zhang, B.; Song, W.; Xie, Q.; Chang, X.; Zhao, R. Forest Canopy Height Estimation by Integrating Structural Equation Modeling and Multiple Weighted Regression. *Forests* **2024**, *15*, 369. [CrossRef]
5. Solberg, S.; Astrup, R.; Gobakken, T.; Næsset, E.; Weydahl, D.J. Estimating spruce and pine biomass with interferometric X-band SAR. *Remote Sens. Environ.* **2010**, *114*, 2353–2360. [CrossRef]
6. Fu, H.; Zhu, J.; Wang, C.; Li, Z. Underlying topography extraction over forest areas from multi-baseline PolInSAR data. *J. Geod.* **2018**, *92*, 727–741. [CrossRef]
7. Huang, H.; Liu, C.; Wang, X.; Biging, G.S.; Chen, Y.; Yang, J.; Gong, P. Mapping vegetation heights in China using slope correction ICESat data, SRTM, MODIS-derived and climate data. *ISPRS J. Photogramm. Remote Sens.* **2017**, *129*, 189–199. [CrossRef]
8. Solberg, S.; Hansen, E.H.; Gobakken, T.; Naessset, E.; Zahabu, E. Biomass and InSAR height relationship in a dense tropical forest. *Remote Sens. Environ.* **2017**, *192*, 166–175. [CrossRef]
9. Zhang, T.; Fu, H.; Zhu, J.; Lopez-Sanchez, J.M.; Gómez, C.; Wang, C.; HeLiu, W. Estimation of Canopy Height from a Multi-SINC Model in Mediterranean Forest with Single-baseline TanDEM-X InSAR Data. *IEEE J. Sel. Top. Appl. Earth Obs. Remote Sens.* **2024**, *17*, 5484–5499. [CrossRef]
10. Cloude, S.R. *Polarisation: Applications in Remote Sensing*; Oxford University Press: New York, NY, USA, 2009.
11. Cloude, S.R.; Papathanassiou, K.P. Polarimetric SAR interferometry. *IEEE Trans. Geosci. Remote Sens.* **1998**, *36*, 1551–1565. [CrossRef]
12. Papathanassiou, K.P.; Cloude, S.R. Single-baseline polarimetric SAR interferometry. *IEEE Trans. Geosci. Remote Sens.* **2001**, *39*, 2352–2363. [CrossRef]
13. Treuhaft, R.N.; Moghaddam, M.; van Zyl, J.J. Vegetation characteristics and underlying topography from interferometric radar. *Radio Sci.* **1996**, *31*, 1449–1485. [CrossRef]
14. Treuhaft, R.N.; Siqueira, P.R. Vertical structure of vegetated land surfaces from interferometric and polarimetric radar. *Radio Sci.* **2000**, *35*, 141–177. [CrossRef]
15. Zou, B.; Zhang, L.; Wang, W.; Sun, D. Forest parameters inversion using PolInSAR data based on genetic algorithm. *Proc. IEEE IGARSS'06* **2006**, *2651*, 2654.
16. Lopez-Sanchez, J.M.; Ballester-Berman, J.D.; Marquez-Moreno, Y. Model limitations and parameter-estimation methods for agricultural applications of polarimetric SAR interferometry. *IEEE Trans. Geosci. Remote Sens.* **2007**, *45*, 3481–3493. [CrossRef]
17. Zhang, Q.; Ge, L.; Hensley, S.; Metternicht, G.I.; Liu, C.; Zhang, R. PolGAN: A deep-learning-based unsupervised forest height estimation based on the synergy of PolInSAR and LiDAR data. *ISPRS J. Photogramm. Remote Sens.* **2022**, *186*, 123–139. [CrossRef]
18. Xing, C.; Wang, H.; Zhang, Z.; Yin, J.; Yang, J. A Review of Forest Height Inversion by PolInSAR: Theory, Advances, and Perspectives. *Remote Sens.* **2023**, *15*, 3781. [CrossRef]
19. Cloude, S.R.; Papathanassiou, K.P. Three-stage inversion process for polarimetric SAR interferometry. *IEE Proc. Radar Sonar Navig.* **2003**, *150*, 125–134. [CrossRef]
20. Kugler, F.; Koudogbo, F.; Gutjahr, K.; Papathanassiou, K. Frequency effects in Pol-InSAR forest height estimation. In Proceedings of the European Conference on Synthetic Aperture Radar (EUSAR), Berlin, Germany, 16–18 May 2006; pp. 1–4.
21. Garestier, F.; Dubois-Fernandez, P.C.; Papathanassiou, K.P. Pine forest height inversion using single-pass X-band PolInSAR data. *IEEE Trans. Geosci. Remote Sens.* **2007**, *46*, 59–68. [CrossRef]
22. Dubois-Fernandez, P.C.; Souyris, J.C.; Angelliaume, S.; Garestier, F. The compact polarimetry alternative for spaceborne SAR at low frequency. *IEEE Trans. Geosci. Remote Sens.* **2008**, *46*, 3208–3222. [CrossRef]
23. Hajnsek, I.; Kugler, F.; Lee, S.K.; Papathanassiou, K.P. Tropical-forest-parameter estimation by means of Pol-InSAR: The INDREX-II campaign. *IEEE Trans. Geosci. Remote Sens.* **2009**, *47*, 481–493. [CrossRef]
24. Chen, H.; Cloude, S.R.; Goodenough, D.G. Forest canopy height estimation using Tandem-X coherence data. *IEEE J. Sel. Top. Appl. Earth Obs. Remote Sens.* **2016**, *9*, 3177–3188. [CrossRef]

25. He, W.; Zhu, J.; Lopez-Sanchez, J.M.; Gómez, C.; Fu, H.; Xie, Q. Forest Height Inversion by Combining Single-Baseline TanDEM-X InSAR Data with External DTM Data. *Remote Sens.* **2023**, *15*, 5517. [CrossRef]
26. Zhang, B.; Fu, H.; Zhu, J.; Peng, X.; Xie, Q.; Lin, D.; Liu, Z. A Multibaseline PolInSAR Forest Height Inversion Model Based on Fourier-Legendre Polynomials. *IEEE Geosci. Remote Sens. Lett.* **2021**, *18*, 687–691. [CrossRef]
27. Zhang, B.; Fu, H.; Zhu, J.; Peng, X.; Lin, D.; Xie, Q.; Hu, J. Forest Height Estimation Using Multi-Baseline Low-Frequency PolInSAR Data Affected by Temporal Decorrelation. *IEEE Geosci. Remote Sens. Lett.* **2020**, *19*, 1–5.
28. Cloude, S.R. Robust parameter estimation using dual baseline polarimetric SAR interferometry. In Proceedings of the IEEE International Geoscience and Remote Sensing Symposium, Toronto, ON, Canada, 24–28 June 2002; Volume 2, pp. 838–840.
29. Lee, S.K.; Kugler, F.; Papathanassiou, K.; Hajnsek, I. Multibaseline polarimetric SAR interferometry forest height inversion approaches. In Proceedings of the ESA POLinSAR Workshop, Frascati, Italy, 24–28 January 2011.
30. Denbina, M.; Simard, M.; Hawkins, B. Forest height estimation using multibaseline PolInSAR and sparse lidar data fusion. *IEEE J. Sel. Top. Appl. Earth Obs. Remote Sens.* **2018**, *11*, 3415–3433. [CrossRef]
31. Lavalle, M.; Shiroma, G.; Hensley, S.; Hawkins, B.; Michel, T.; Muellerschoen, R.; Zheng, Y.; Simard, M.; Pinto, N.; Lou, Y. First Results of Vegetation Height Retrieval from the 2016 UAVSAR AfriSAR Campaign. ESA PolInSAR Workshop. 2017. Available online: http://seom.esa.int/polinsar2017/files/polinsar2017_d5p3.pdf (accessed on 20 June 2024).
32. Caicoya, A.T.; Kugler, F.; Papathanassiou, K.; Biber, P.; Pretzsch, H. Biomass estimation as a function of vertical forest structure and forest height-Potential and limitations for Radar Remote Sensing. In Proceedings of the 8th European Conference on Synthetic Aperture Radar, Aachen, Germany, 7–10 June 2010; pp. 1–4.
33. Xie, Y.; Fu, H.; Zhu, J.; Wang, C.; Xie, Q. A LiDAR-aided multibaseline PolInSAR method for forest height estimation: With emphasis on dual-baseline selection. *IEEE Geosci. Remote Sens. Lett.* **2019**, *17*, 1807–1811. [CrossRef]
34. Zhu, J.J.; Xie, Q.; Zuo, T.; Wang, C.; Xie, J. Criterion of Complex Least Squares Adjustment and Its Application in Tree Height Inversion with PolInSAR Data. *Acta Geod. Cartogr. Sin.* **2014**, *43*, 45–51.
35. Fu, H.; Zhu, J.; Wang, C.; Xie, Q.; Zhao, R. Polarimetric SAR Interferometry Vegetation Height Inversion Method of Complex Least Squares Adjustment. *Acta Geod. Cartogr. Sin.* **2014**, *43*, 1061–1607.
36. Fu, H.; Wang, C.; Zhu, J.; Xie, Q.; Zhao, R. Inversion of vegetation height from PolInSAR using complex least squares adjustment method. *Sci. China Earth Sci.* **2015**, *58*, 1018–1031. [CrossRef]
37. Lin, D.; Zhu, J.; Fu, H.; Xie, Q.; Zhang, B. A TSVD-based method for forest height inversion from single-baseline PolInSAR data. *Appl. Sci.* **2017**, *7*, 435. [CrossRef]
38. Xie, Q.; Zhu, J.; Wang, C.; Fu, H.; Zhang, B. A S-RVoG model-based PolInSAR nonlinear complex least squares method for forest height inversion. *Acta Geod. Cartogr. Sin.* **2020**, *49*, 1303–1310.
39. Lee, S.K.; Fatoyinbo, T.E.; Lagomasino, D.; Feliciano, E.; Trettin, C. Multibaseline TanDEM-X mangrove height estimation: The selection of the vertical wavenumber. *IEEE J. Sel. Top. Appl. Earth Obs. Remote Sens.* **2018**, *11*, 3434–3442. [CrossRef]
40. Kugler, F.; Lee, S.K.; Hajnsek, I.; Papathanassiou, K.P. Forest height estimation by means of Pol-InSAR data inversion: The role of the vertical wavenumber. *IEEE Trans. Geosci. Remote Sens.* **2015**, *53*, 5294–5311. [CrossRef]
41. Xie, Y.; Fu, H.; Zhu, J.; Wang, C.; Xie, Q.; Wan, J.; Han, W. Improved forest height mapping using multi-baseline low-frequency PolInSAR data based on effective selection of dual-baseline combinations. *Remote Sens. Environ.* **2024**, *312*, 114306. [CrossRef]
42. Zhao, H.; Zhang, T.; Ji, Y.; Zhang, W. Uncertainty analysis for forest height inversion using L/P band PolInSAR datasets and RVoG model over kryclan forest site. *Int. J. Appl. Earth Obs. Geoinf.* **2024**, *130*, 103886. [CrossRef]